

SCNet: A Generalized Attention-based Model for Crack Fault Segmentation*

Hrishikesh Sharma
TCS Research
hrishikesh.sharma@tcs.com

Prakhar Pradhan
TCS Research
prakhar.pradhan@tcs.com

Balamuralidhar Purushothaman
TCS Research
balamurali.p@tcs.com

Abstract—Anomaly detection and localization is an important vision problem, having multiple applications. Effective and generic semantic segmentation of anomalous regions on various different surfaces, where most anomalous regions inherently do not have any obvious pattern, is still under active research. Periodic health monitoring and fault (anomaly) detection in vast infrastructures, which is an important safety-related task, is one such application area of vision-based anomaly segmentation. However, the task is quite challenging due to large variations in surface faults, texture-less construction material/background, lighting conditions etc. Cracks are critical and frequent surface faults that manifest as extreme zigzag-shaped thin, elongated regions. They are among the hardest faults to detect, even with deep learning. In this work, we address an open aspect of automatic crack segmentation problem, that of generalizing and improving the performance of segmentation across a variety of scenarios, by modeling the problem differently. We carefully study and abstract the sub-problems involved and solve them in a broader context, making our solution generic. On a variety of datasets related to surveillance of different infrastructures, under varying conditions, our model consistently outperforms the state-of-the-art algorithms by a significant margin, without any bells-and-whistles. This performance advantage easily carried over in two deployments of our model, tested against industry-provided datasets. Even further, we could establish our model's performance for two manufacturing quality inspection scenarios as well, where the defect types are not just crack equivalents, but much more and different. Hence we hope that our model is indeed a truly generic defect segmentation model.

Index Terms—Semantic Segmentation, Local attention, Infrastructure Monitoring, Data imbalance, Crack Segmentation

I. INTRODUCTION

SEMANTIC Segmentation of anomalous regions on objects of interest is an important vision task, with multiple industrial applications. One such application area is related to infrastructures. *Infrastructures* are facilities and services set up and operated in various nations, to support their economy, industry and living conditions. They are vast man-made objects, whose examples include bridges, dams, rail corridors, tunnels and pipelines, pavements and roads, towers and buildings etc. To maintain their safety, durability and other health parameters during their service life span, it is required that any fault that is developing over time is detected and attended to, via repairs, before it manifests into a widespread catastrophe. Hence *periodic health inspections* of infrastructures, which can detect and quantify faults in a timely manner, are carried out.

These inspections provide aid in prioritizing and planning of maintenance tasks.

There are multi-fold challenges that arise during health inspections. During remote visual surveillance for inspection, due to hazardous and unreachable premises through which infrastructures mostly pass, drones are being increasingly used to perform such surveillance. This mode of surveillance leads to capturing of large volumes of visual data, leading to increasing demand of automated visual analysis. Further, due to safety requirements, the visual data is captured from at least five meters of distance. This leads to nascent fault regions on the infrastructures being imaged as small-sized regions quite often, making their automated segmentation a tough task. The other challenges include types and variations of faults themselves. Many intrinsic variations in various fault regions are in fact *continuous* factors of variations, e.g. region's shape, region's texture etc. For example, both efflorescence and cracks grow into very random shapes. Extrinsic factors of variations mainly arise from outdoor conditions such as lighting condition, surface wetness, occlusion and shadow effect etc. Due to such variations, the fault regions generally display a lack of any obvious region-wide pattern. This is perhaps the biggest challenge in automating visual fault detection.

In terms of impact on structural health, detection of *crack* fault category is known to be a top priority maintenance task. Visually, cracks being extremely thin, highly irregular and long, embedded at arbitrary locations in backgrounds which represent diverse materials and hence textures, they are among hardest to detect in an image (refer Fig. 1). Cracks are known to co-occur along with other faults, such as efflorescence [16], making the classification task multi-target and thus exacerbating their analysis. Given its importance and complexity, a lot of prior research on crack detection has been carried out, in past few decades. Till few years back, crack detection was carried out mainly based on *intensity-based methods*. These methods had the problem of requiring to manually tune various parameters such as thresholds to deal with different lighting conditions etc. Hence the applicability and reliability of these methods was limited. In recent years, deep learning (DL-)based methods operate by making task-specific decisions by looking at a larger context hierarchically. Hence they have demonstrated much better performance in computer vision as well as many other domains. The DL-based methods for crack detection broadly fall in two categories. *Semantic*

*To appear in ICVGIP'21



Fig. 1: Example Crack Regions in Infrastructures, annotated with Yellow-colored pixels

Segmentation(pixel-level classification) approach is preferred over patch-based classification for crack detection, because it enables robust downstream task of crack mechanical analyses. Such downstream analyses can be further used to predict crack growth over time [39], [27]. Our literature study showed that the prior semantic segmentation methods have been mostly biased towards usage of a single crack dataset, more often being a road/pavement dataset, as is also corroborated in [18]. Their affinity towards one dataset introduces implicit bias, leading to overfitting that limits their effectiveness. In another words, given multiple factors of variations inherent in faults of various nature as described earlier, these methods are unable to cope with the *domain shift* between different datasets.

In this paper, we take a different approach towards the problem of semantic segmentation of crack regions. We find out important **generic** sub-problems, which occur not only in crack segmentation task, but also in other non-crack vision tasks, sometimes occurring beyond even semantic segmentation. Some examples include, as will be explained in section III, usage of attention to compensate for lack of contextual information, dealing with class imbalance etc. When we solve these sub-problems in a *broader* context, we are able to get the required generalizability across surveillance scenarios, as well as *consistent* improvement in performance, in terms of F1 score and area under P-R curve(AUPRC). We prove our approach’s effectiveness and portability over multiple datasets, arising out of multiple industrial contexts and different infrastructures, and as a bonus, two manufacturing scenarios as well.

To summarize, our proposed method has the following

contributions:

- We design a new soft attention mechanism, to be used in the multi-scale feature space.
- We carefully use a novel multi-task combination of binary focal loss and softIoU loss to simultaneously handle class imbalance sub-problem as well as reduce the pixel-level shift in the prediction.
- We generate and additionally input a noisy *prior* about crack region, which improves performance.

The rest of this paper is organized as follows. We summarize the related prior research in section II. In section III, we present design details of SCNet model, as well as solutions to the broader sub-problems within. It is followed by overview of datasets used in this paper, in section IV. The results and performance of SCNet is presented in section V. We present a detailed ablation study to highlight the importance of various design factors in section VIII, before we conclude the paper.

II. RELATED WORK

Here, we provide brief overview of recent advances in research on topics that are relevant to our problem.

A. Vision-based Crack Detection

Crack detection has been the mainstay of research on visual surveillance of faults in infrastructures, over last many decades. Its applicability has been researched upon in variety of application scenarios: tunnel safety inspection [61], [38], dam safety inspection [9], rail corridor inspection [52], steel bridges [22], [14], concrete bridges [16], mine safety [11],

pavement crack detection [18], [25], building safety inspection [8], to name a few. The techniques for detection belong to two phases. For prior methods which do not employ deep learning, see comprehensive literature survey in [59]. While very recently sporadic deep generative modeling based approaches have started appearing [6], almost all the deep learning based approaches in last few years have been supervised discriminative approaches, for obvious reasons. These DL-based discriminative approaches can further be grouped into two important categories.

1) *Classification-based Approaches*: The initial DL-based approaches were patch-level classification approaches [29], [19], [49], [48], [47],[15], [3], [10], due to smaller datasets. Usage of patches instead of whole images allowed having more training data. However, the performance of these methods was average.

2) *Segmentation-based Approaches*: More recently, with appearance of larger crack datasets on variety of surfaces, the research community has focused upon more fine-grained detection task, via semantic segmentation [32], [23], [41], [11], [50], [2]. As mentioned earlier, we too follow this approach, and design to get a versatile solution.

B. Semantic Segmentation

Starting from earlier important works such as SegNet and FCN, there have been many important advances on the task of semantic segmentation. Usage of multi-scale context [53] and careful architecture design are main concerns of segmentation. Many architectures resemble an autoencoder-style hourglass architecture, with the recent U-Net [58] being quite popular. As motivated in FCN, all recent important architectures are fully convolutional, and use residual propagation. For a more in-depth survey of recent segmentation approaches, see [37].

The main limitation of these approaches is that they are designed for segmentation of non-anomalous scenes such as CityScapes, Kitti, organs in biomedical images etc. As is known, CNNs are biased towards learning texture [36], while surfaces of infrastructures are mostly texture-less e.g. steel, concrete etc. [64]. Hence the naive applicability of established methods is quite poor, as we also found experimentally.

C. Attention Mechanism

Attention mechanism is an attempt to mimic human brain's ability to selectively concentrate on relevant objects, while ignoring rest of the scene and the objects. At few times, such relevant objects relate to anomalies: our brain is able to effortlessly localize an abnormal aspect/region within a scene. The recent breakthrough modeling of attention happened in NLP area, wherein different parts of contextual information are selectively weighted using learnt weights, to attend and highlight the (current) input token. This mechanism was first adapted in computer vision in [54], with weighting over various regions of background/context. This became the foundation of most of the future attention-based solutions to vision tasks. Recently, attention mechanism was also adopted in various semantic segmentation approaches [46], [20], [26], [53]. The approach

in [26] is closest to ours approach in solving one sub-problem. However, while they focus on learning pixel-specific attention masks based on spatial distance in input image, to implement non-local attention, we focus on learning attention masks in the pyramidal feature space (scale-specific attention), for a reason described in section III-A. This focus is also the reason behind our work being more precise than [4], [7], [1], where attention modules are used in the residual paths.

III. SCNET MODEL

We model the problem as a segmentation of foreground crack region vs. rest of background region. We take a **Supervised** approach, rather than an unsupervised approach, since it is indicated in a path-breaking work [17] that whenever sufficient ground truth annotations are available, supervised approaches are still likely to outperform unsupervised approaches on downstream tasks. The architecture part of our model is an extension of the well-known and well-performing (supervised) UNet segmentation model [58]. Much like instance segmentation, where generation of foreground mask is a primary concern, here our concern is to focus upon and predict a crack mask only. Unlike instance segmentation, where we found that the poor concurrent prediction of crack bounding boxes, which are very foreground-sparse, pulls down the performance of mask generation as well, in a multi-task learning setup, here we focus on pixel-level prediction via a *semantic segmentation* task. In the **Supervised CrackNet** (SC-Net) design, we solve the following important sub-problems carefully, not addressed in the baseline or elsewhere.

A. Discriminative Crack Representation

Cracks, like many other anomalies, are *local phenomenon*, occurring randomly on a surface at any location. Hence there is no useful global cue for their localization, in the pixel space. Instead of such cue, we turn to attention mechanism to enhance the likelihood of a pixel being classified into a foreground pixel. Our novel attention module enables the encoder to learn a foreground representation, which is more discriminative towards surface faults including cracks.

It was brought out in FCN that different stages of the convolutional layers within the encoder bring out diverse information about the objects. More specifically, [62] showed that first layer learns edge-like artefacts, second layer learns contours and corners, and so on. Thus, the features of lower layers mostly represent structure information, while the features of deeper layers mostly represent shape/semantic information of a region. Cracks being thin regions with random shapes which absorb light and are dark, any useful representation of them has to weigh more on the structural aspect of it. Hence we employ *attention operator in the scale-space* naturally implied within the feature pyramid of an encoder, to implement such relative weighting. This relative weighting is applicable to segmentation of cracks irrespective of the surface on which they appear, lending it the required *generality*.

Our design of scale-space attention operator works convolutionally over a block of feature maps, F , of size $H \times W \times C$.

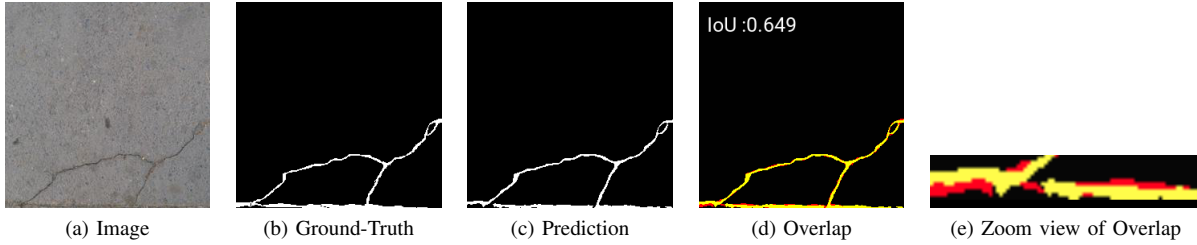


Fig. 2: Disproportional degradation of IoU measure w.r.t. minor shift in predicted segmentation. Yellow: Predicted Crack Pixels; Red: GT Crack Pixels

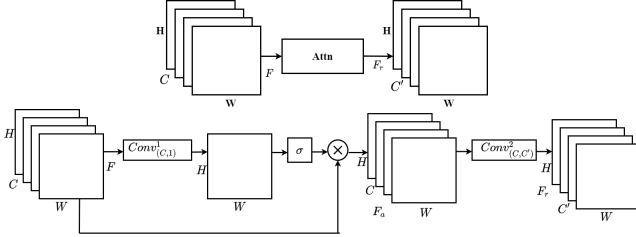


Fig. 3: Scale-wise Attention Module Structure

As shown in Fig. 3, in this design, we do not use any pooling mechanism. The intuition is that the foreground being highly imbalanced as compared to background, there is not much information in the feature maps, and any kind of pooling will further trivialize the feature information contained in the feature maps, leading to decreased performance. We could corroborate this using experiments later. The attention masks so generated are multiplied with the original feature maps, F , to get intermediate feature maps, F_a , as per general practice. We experimentally found that using an additional convolutional layer, $Conv^2_{(C,C')}$ over F_a , gives more refined feature maps, F_r which further enhance the performance of the model. To summarize,

$$\begin{aligned} F_a &= \sigma \left(Conv^1_{(C,1)}(F) \right) \times F \\ F_r &= Conv^2_{(C,C')}(F_a) \end{aligned} \quad (1)$$

where σ is the sigmoid activation function, \times denotes the element-wise multiplication and $Conv_{(m,n)}$ denotes a convolutional layer with m number of input channels and n number of output channels. We embed our novel attention operator in the feature pyramid, in the same way as [28].

B. Minimizing FPs from Reconstruction-based blur

Using attention only in the scale space of the encoder improves the true positives, but leads to many pixels being misclassified as false positives (FPs), especially near ground truth (GT) boundaries. Our interpretation is that this happens due to well-known problem of additional blur in autoencoder-style reconstructions [35] (our architecture resembles autoencoder-style hourglass architecture). Cracks being highly imbalanced

foregrounds, ignoring false positives leads to drastic fall in segmentation performance. To ameliorate this situation, we symmetrically use attention modules in decoder as well. Such usage indeed led to significant drop in amount of pixel-wise false positives, once again across a diverse set of surfaces.

C. Reducing Impact of Class Imbalance

Cracks being thin, elongated objects (sometimes 3-5 pixels wide [9]), the ratio of crack pixels vs. non-cracks pixels (refer Table II) is quite low. This leads to *severe* class imbalance in training data. Learning effective classifiers in presence of class imbalance, which do not trivially misclassify foreground into background, is a long-researched topic in machine learning. Among all known ways to tackle *severe* class imbalance, we employ a pixel-wise adaptation of focal loss to learn an effective classifier. **Focal loss** was recently proposed in context of object detection task, to train a bounding box classifier in presence of severe imbalance [45], but its design is generic. As ablation studies show, usage of focal loss in place of binary cross-entropy loss *with* median frequency balancing, systematically reduced the negative impact of imbalance across all datasets. We also tried to use another recent loss-based approach to tackle imbalance, the Dice loss [42], but usage of focal loss was found much superior to this loss.

D. Tighter Alignment of Predictions to GT Regions

We empirically found out one more reason for limited performance of existing crack segmentation models: poor localization. As is shown in Fig. 2, even after using attention and handling class imbalance, the predicted crack region was found to be offset by few pixels against the ground truth (GT). Cracks being very thin regions, few pixels' shift, especially in the direction perpendicular to its approximate major axis of its axis-aligned bounding box, leads to non-trivial fall in overlap, a localization measure. The most popular overlap measure is intersection-over-union (IoU), but is non-differentiable. To reduce the above fall, we employed and tested various approximations of IoU as an auxiliary loss, designed for usage in semantic segmentation task. Specifically, we implemented and used Lovász loss [40], Soft-IoU loss [44] and NeuroIoU loss [31]. As is shown in Table X, usage of Soft-IoU loss gave us relatively better performance improvement. We then used soft-IoU loss in conjunction with pixel-wise focal loss, in a

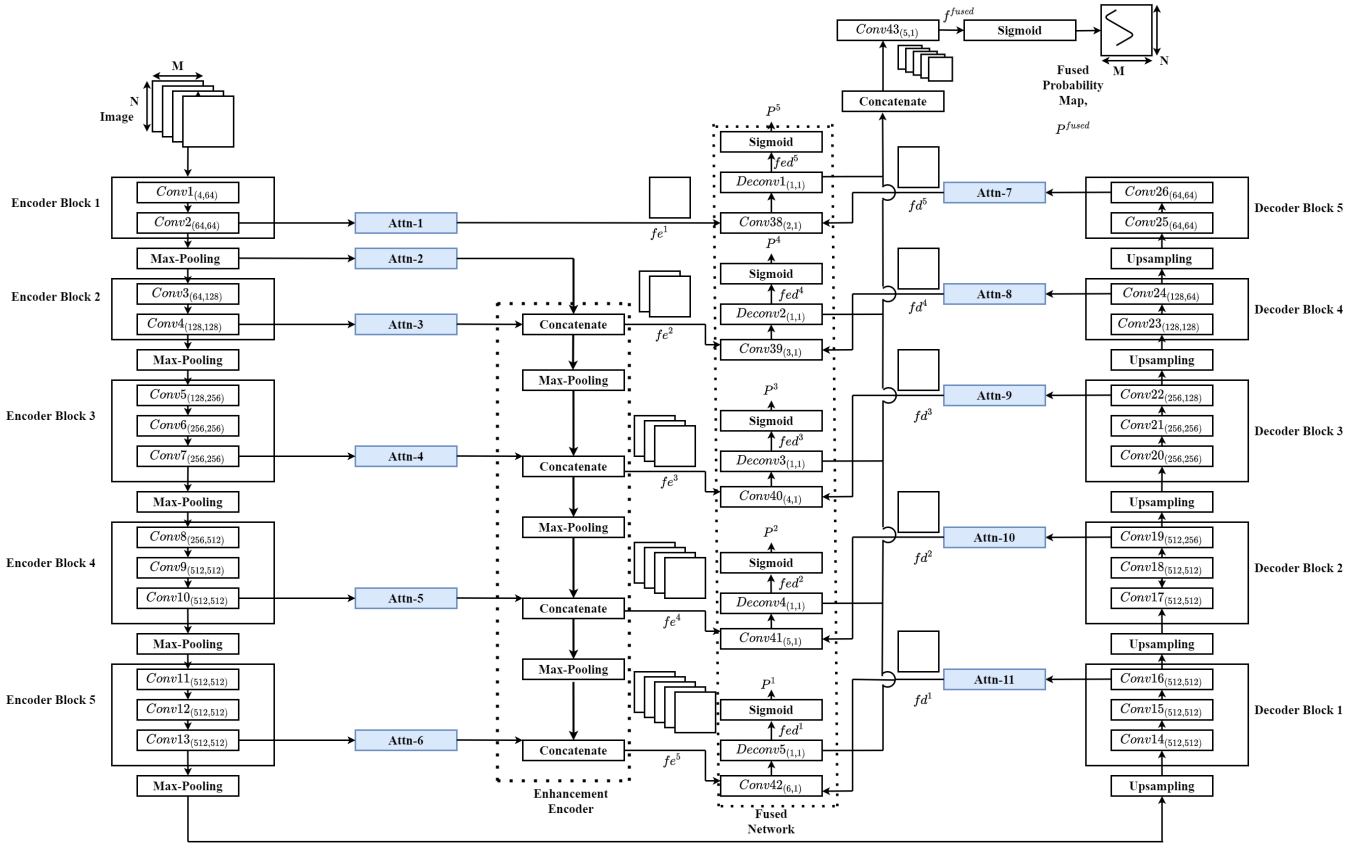


Fig. 4: SCNet Architecture

multi-task learning setup, as in Eq. 6. As is shown in [34], not all tasks can work advantageously together, in a MTL setup. However, it is known from research over object detection that a classification and a regression loss supplement each other quite well, in box prediction task. We found the same synergistic effect of these losses in pixel-level prediction task as well.

E. Biasing with a Prior

Since cracks resemble morphologically dilated edges of various shapes, we also experimented with biasing the input with a location prior, using edges. Specifically, we used the popular HED algorithm [55] to generate a noisy edge map. We then use the edge map in a different way, by adding it as an additional channel to the RGB input. Introduction of additional channel led to marginal improvement in performance, across various datasets.

F. Overall Architecture

The proposed architecture is built on an extension of UNet called HCNN [13], and hence has an hourglass architecture. Such structure results in somewhat sharper reconstruction of object boundaries [33]. The network, as shown in Fig. 4, consists of 4 sub-networks, attention based encoder, attention-based decoder, enhancement encoder and a fused network.

The **encoder** follows the VGG-C [56] network architecture, containing 5 encoder blocks with 13 convolutional layers

placed sequentially. Usage of max pooling instead of dilated convolution helps us to retain the max pooling indices, and transfer subsequently to the decoder, helping to recover the loss of details in the representation space. The feature maps output by each encoder block are further passed through the attention modules (Fig. 3), to focus on the crack regions within them.

The **enhancement encoder** is used to improve the feature maps from the deeper encoder blocks. The purpose of performing iterative fusion of feature maps from successive encoder blocks, within this sub-network, is explained in [13].

The attention-driven **decoder** is used in the network, for reconstructing the crack region from focused feature maps. It performs bilinear interpolation-driven upsampling to decode the region from the latent feature space representation. Specifically, the upsampling incorporates the pooling indices transferred by the encoder, to perform *non-linear* upsampling.

In the **fused** sub-network, feature maps from the enhancement encoder and decoder at the corresponding scale are fused using a 1×1 convolutional module. The output of the convolutional module is then up-sampled to the input image size and passed through sigmoid activation to calculate the predicted probability maps at each stage. There are thus 5 predicted probability maps. To obtain a final fused probability map, the feature maps, f_{ed}^i from each scale are concatenated and

passed through a convolutional module and sigmoid activation function. The probability map so obtained, is passed through an iterative thresholding process [18] to obtain a binary crack probability map. In the complete network, the feature maps are concatenated along the channel dimension.

The entire SCNet model, and the sub-networks within, can be mathematically described by a system of equations. For one example sub-network, e.g. fused network, the equations that represent the generation of the final fused probability map are shown as follows.

$$\begin{aligned} f_{ed}^5 &= Deconv1_{(1,1)}(Conv38_{(2,1)}(Concat(f_e^1, f_d^5))) \\ f_{ed}^4 &= Deconv2_{(1,1)}(Conv39_{(3,1)}(Concat(f_e^2, f_d^4))) \\ f_{ed}^3 &= Deconv3_{(1,1)}(Conv40_{(4,1)}(Concat(f_e^3, f_d^3))) \\ f_{ed}^2 &= Deconv4_{(1,1)}(Conv41_{(5,1)}(Concat(f_e^4, f_d^2))) \\ f_{ed}^1 &= Deconv5_{(1,1)}(Conv42_{(6,1)}(Concat(f_e^5, f_d^1))) \end{aligned} \quad (2)$$

Each encoder block, and units in other block at same horizontal level, together signify i^{th} scale. Let P^i denote the pixel-wise probability map obtained at i^{th} scale in the fused sub-network, and P^{fused} denote the final fused probability map. Then,

$$P^i = \frac{1}{1 + e^{-f_{ed}^i}} \quad (3)$$

$$f^{fused} = Conv43_{(5,1)}(Concat(f_{ed}^5, f_{ed}^4, f_{ed}^3, f_{ed}^2, f_{ed}^1)) \quad (4)$$

$$P^{fused} = \frac{1}{1 + e^{-f^{fused}}} \quad (5)$$

where $Conv_{(m,n)}$ denotes a convolutional layer, with m number of input channels, and n number of output channels.

G. Loss Formulation

To handle per-pixel classification with class imbalance, along with perceived shift in predicted region, we use a novel combination of binary focal loss and Soft-IoU loss in a *multi-task learning* setup. Further, to enhance the probability of true classification, contribution of predictions from the individual scales is also factored in the overall loss, a form of *deep supervision*.

Let the training dataset consist of K (image, ground-truth) pairs, $\{(X^k, Y^k), k = 1, 2, \dots, K\}$, where, $Y^k = \{y_j^k, j = 1, 2, \dots, M \times N, y_j^k \in \{0, 1\}\}$. Let L_i^{focal} denote the focal loss at the i^{th} stage, computed using f_{ed}^i . Also, let L_{focal}^{fused} denote the focal loss calculated using the f^{fused} . Similarly, let L^{IoU} denote the Soft-IoU loss calculated using the fused probability map P^{fused} . Then, the overall loss can be computed as

$$L_{focal}^{total} = L_{focal}^{fused} + \sum_{i=1}^5 w_i * L_{focal}^i \quad (6)$$

$$L_{focal}^i = \sum_{j=1}^{MN} \ell_1(f_j^i, y_j) \quad (7)$$

$$L_{focal}^{fused} = \sum_{j=1}^{MN} \ell_1(f_j^{fused}, y_j) \quad (8)$$

$$L_{focal}^{total} = \sum_{j=1}^{MN} \ell_1(f_j^{fused}, y_j) + \sum_{j=1}^{MN} \sum_{i=1}^5 w_i * \ell_1(f_j^i, y_j) \quad (9)$$

$$L^{IoU} = \ell_2(P^{fused}, Y) \quad (10)$$

$$L_{total} = L_{focal}^{total} + L^{IoU} \quad (11)$$

where w_i are scalar weights used to give relative importance, ℓ_1 is focal loss function defined in [45] and ℓ_2 is Soft-IoU loss function defined in [44].

IV. DATASETS

As specified earlier, we have targeted our model design for versatility as well as acceptably high performance. To verify the effectiveness of design, we have carefully chosen a group of datasets to benchmark the performance. The choice is driven by the consideration of their *heterogeneity and size*. We have also taken different deployment scenarios into consideration: aerial/drone-based as well as terrestrial, again to prove effectiveness across various deployment scenarios. Some primary statistics about the datasets are as in Table I. For few datasets, which did not provide an explicit test set, we held out 20% of images for testing the model. The individual details of each dataset can be found in the corresponding papers, cited within first column. Two datasets arising out of industrial deployment scenarios are listed in last two rows, and do not have any corresponding papers.

TABLE I: Summary of Public Datasets Used

Name	Infrastructure	Size (crack samples)
Deepcrack [18]	Pavements	1953
CODEBRIM ¹ [16]	Bridges	2281
METU [24]	Building Facade	12115
CrackForest [50]	Road Images	323
Wessex Water	Water Pipeline Inner Walls	4874
BMW	Road Images	5892

V. EXPERIMENTS AND RESULTS ON PUBLIC DATASETS

In this section, we demonstrate our goal of achieving versatility and improvement in performance, by a set of carefully designed experiments. We test our model from both semantic segmentation and anomaly detection point of views, since crack is also a surface anomaly and occurs as a rare spatial event. We have tested our model without any bells-and-whistles, especially CRF-based post-processing that is commonly used in certain semantic segmentation networks.

¹Additional region-wise annotations are available from [12]

A. Implementation

We implemented SCNet model using PyTorch. All the weights and biases have been initialized using Xavier initialization. We used SGD [63] as the optimization technique for the model training. The size of the input images is 256×256 , while the mini-batch size used is 4. We used an initial learning rate of 0.0001, with momentum value of 0.9, and weight decay of $2e - 4$. The relative weights assigned to both focal loss and Soft-IoU loss in 11 is 1.0. The α and γ used in the focal loss are 1.0 and 2.0 respectively. To further enhance the training process, the RGB pixel values of the input image is normalized between -1 and $+1$. The scalar weights used in the equation 6 to give relative importance in the final prediction are $\langle 0.5, 0.75, 1.0, 0.75, 0.5 \rangle$ respectively. For the attention mechanism in eq. 1, we empirically found $C' = 1$ giving best performance. The input image to the network is a 4 channel image, where the fourth channel is a binary edge map of the RGB image. To compute the binary edge map, we used a public implementation of HED [30].

B. Data Augmentation

To achieve fair comparison with the baseline [13], we followed similar data augmentation process as used in [13], rotating the images from 0 to 90 degrees, flipping the image horizontally and vertically, randomly cropping the flipped images with a size of 256×256 . The percentage of crack and non-crack pixels for each dataset after data augmentation is quoted in the Table II, which shows the existence of severe data imbalance problem.

TABLE II: Degree of Class Imbalance in Datasets

Name	Crack Pixels (%)	Non-crack Pixels (%)
Deepcrack [18]	4.68	95.31
CODEBRIM [16]	3.78	96.21
METU [24]	7.02	89.47
CrackForest [50]	3.04	96.95
Wessex Water	6.78	93.22
BMW	11.63	88.37

C. Evaluation Metric

We report the pixel-wise **F1 score** of the crack class, as the primary evaluation metric. Both the false positives and true negatives are identified with respect to crack pixels only, since we are interested in segmentation of the lone foreground class. To compute this score, we use an iterative thresholding process [18] over P^{fused} . The iterative thresholding can be seen as computing the maximum F1 score via *finite* sampling of the corresponding P-R Curve. A very similar metric which considers both FPs and TNs is IoU of the foreground class. Though we only report the more popular figure in literature on this problem, F1 score, we also measured the IoU metric. The trends in IoU performance are **fully consistent** in the sense that on all datasets, SCNet performs the best by a fair margin. From another angle, though crack is an anomaly, and area

under Receiver Operating Curve (ROC) is a popular metric in anomaly detection, for binary classification under extreme imbalance scenarios, PRC is used instead of ROC for reasons described in [57]. Hence we report both PRC and F1 score in next section.

There are circumstances when one has to evaluate and compare against both patch-based and pixel-based semantic segmentation models, as in [51]. Where we have to similarly compare against patch-based classification, we approximately convert our pixel-wise metric into *region-wise F1 score* of 32×32 -sized patches. In a ground-truth image, X , a patch is said to have a crack, when the number of crack pixels in the patch constitutes at least 5% of the total pixels (number based on statistics in Table II). For the predicted probability map, a region is said to have a crack, when the model can correctly detect at least 50% of the crack pixels. Then the region-wise F1 score can be calculated by finding out true positive, false positive and false negative patches.

$$Precision_{patch-wise} = \frac{TP_{\#patches}}{TP_{\#patches} + FP_{\#patches}} \quad (12)$$

$$Recall_{patch-wise} = \frac{TP_{\#patches}}{TP_{\#patches} + FN_{\#patches}} \quad (13)$$

$$F1_{patch-wise} = \frac{2 \times Prec_{patch-wise} \times Rec_{patch-wise}}{Prec_{patch-wise} + Rec_{patch-wise}} \quad (14)$$

TABLE III: Comparative Pixel-wise F1 Scores

Dataset	DC-1[18]	HCNN (Baseline)	DC-2[25]	SCNet (Ours)
Deepcrack	85.2	87.6	86.2	91.23
CODEBRIM	60.7	57.9	54.2	64.22
METU	66.10	65.40	57.80	69.13
CrackForest	84.42	79.91	79.58	90.40

D. Quantitative Performance

For each shortlisted dataset, we have chosen to compare against those state-of-the-art models, whose reported performance could be reproduced. In some cases, we had to do our own implementation of such models carefully². Another concern was that the evaluation metric used by various papers is quite varied, so not all works were comparable on our evaluation metric of choice³. It so turns out that we could reproduce results having the chosen F1 score metric, of three models. Two of these models are *natively* associated with two shortlisted datasets, and are introduced in the corresponding (dataset) paper. Hence, we used these three *recent* models, and along with our model, re-trained and evaluated their

²The baseline HCNN model was reimplemented by us, since code was unavailable.

³Prominent omission for this reason is MetaQNN model used by CODEBRIM

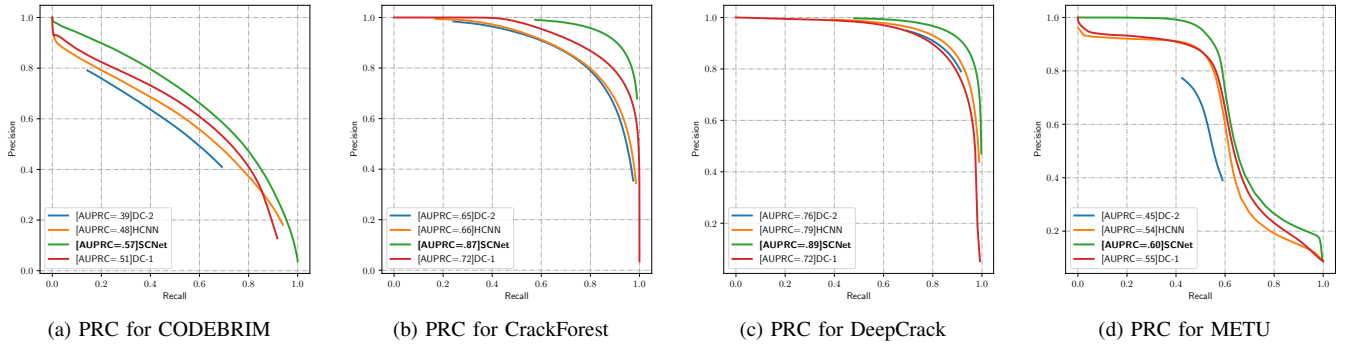


Fig. 5: P-R Curve and AUPRC of various models, on each dataset

performance on all four datasets. The F1 scores are shown in Tables III and IV. It can be clearly observed from these tables that our model outperforms other models, on **all** datasets, in terms of F1 score. The *minimum advantage* on pixel-wise F1 score is 4.09% (on Deepcrack dataset), though in general it gives much higher advantage on other datasets and deployment scenarios. On patch-wise F1 score, our model outperforms state-of-the-art by quite a significant margin.

TABLE IV: Comparative Region-wise F1 Scores

Dataset	Patch-based Classification	SCNet(ours)
Deepcrack	62.53	97.03
CODEBRIM	38.67	74.69
METU	47.74	77.48
CrackForest	66.84	96.62

Figures 5a, 5b, 5c and 5d show the *Precision-Recall* curves of each model, on each dataset. The figures also provide the AUPRC value for each model, per dataset. Given the very small % of foreground class pixels as baseline AUPRC per dataset (refer Table II), it is obvious that though all models have robust AUPRC for the foreground when compared to the baseline, our model has the best AUPRC among all models, on *each* dataset. Notably, for same precision, we have better recall value among models. This in turn can be attributed to reduction in missed detections in general, due to usage of attention mechanism. Lesser missed detection is something that is most sought after, in anomaly detection problems, where anomalies are rare.

TABLE V: Cross-datasets Performance of SCNet

Trained On	Tested On			
	Deepcrack	CrackForest	Codebrim	METU
Deepcrack	91.23	63.59	42.14	58.45
CrackForest	64.89	90.4	42.38	57.2
Codebrim	63.08	63.64	64.22	56.79
METU	65.78	64.48	51.32	69.13

E. Qualitative Performance

The qualitative performance of each model, against a representative input belonging to each dataset, can be seen in Fig. 6. Each column depicts the prediction output (including one column for ground truth), while each row names the dataset to which the each different input image belongs to. It can be seen that predictions of our model are more close to the GT, than other models.

F. Discussion

To understand how our model provides the required performance, we hereby provide and explain a series of visualizations. The contribution of individual scales in the final prediction has been shown in Fig. 7, using probability maps P^i . It is clear from this figure that all scales in the network try to capture crack-like structures in the image. Further, the probability maps from the shallower stages contribute more in the final prediction, as is expected and explained in section III-A. To understand deeper about performance at each scale, Fig. 8 shows the visualization of the attention maps learnt at each scale of the encoder, by the corresponding attention module. Two important aspects become clear from these attention maps. One, in lack of any obvious texture in background, the attention module makes crack pixels provide contextual support among themselves, to boost their classification probability. Two, the attention maps generated by deeper encoder stages also produce sharp and significant contextual attention, thereby being relevant to the model design even when the corresponding probability maps were found by us to be diffused a bit, as in Fig. 7. The variation in these attention maps justifies the use of multiple attention modules, one at each scale, rather than a single attention module at the end of the encoder, as is the case with architectures of many a popular attention-based segmentation architectures, e.g. [21], [20].

To test the low-data adaptability property of our model, we tested SCNet in a *transfer learning* setup. Briefly, we trained the model on one dataset, and tested it on another. The results are tabulated in Table V. It can be seen that our model is able

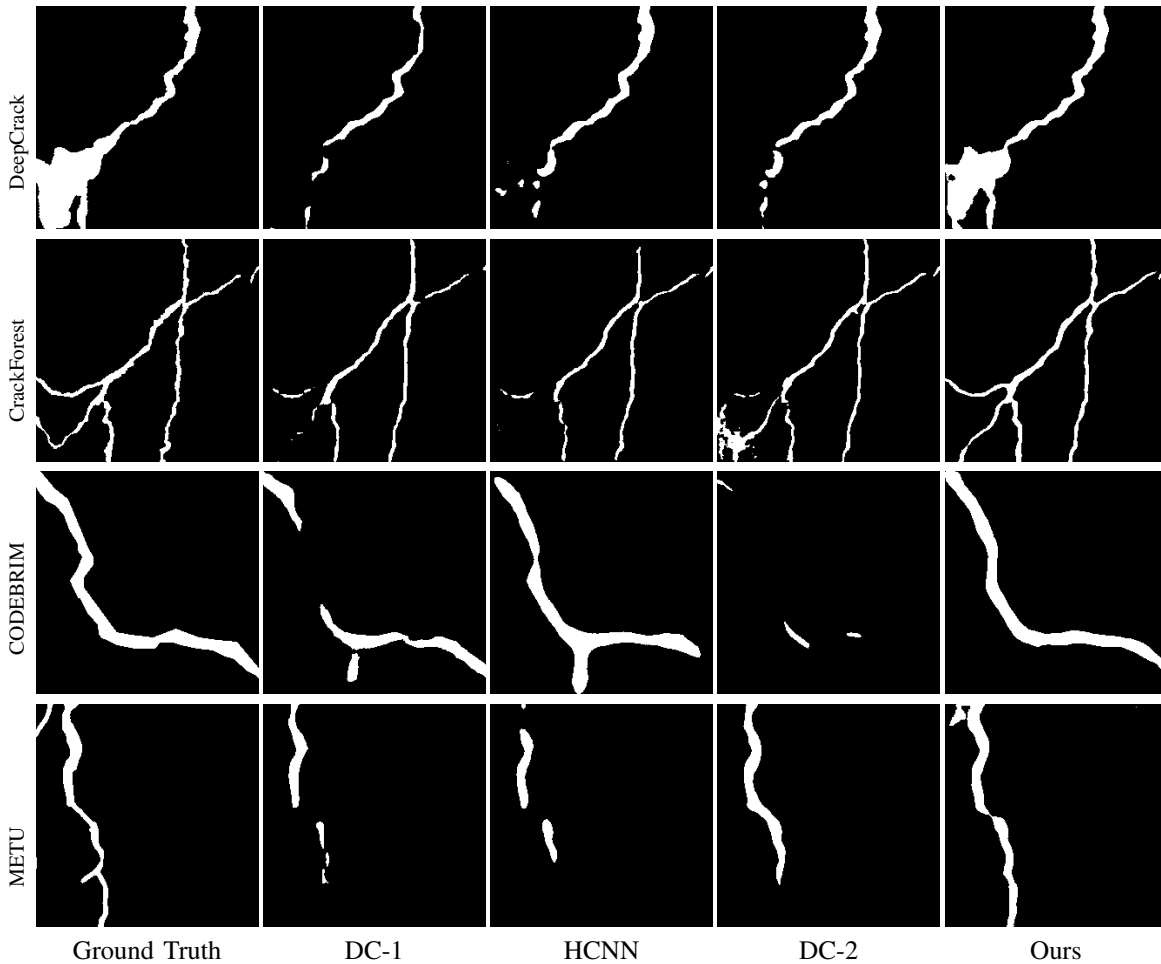


Fig. 6: Qualitative Comparison of Segmentation Results, across Models and Datasets

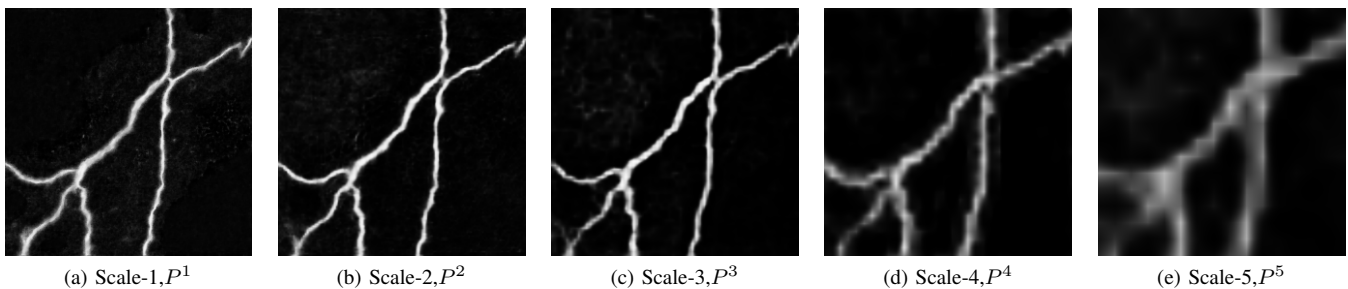


Fig. 7: Visualization of Predicted Probability maps at each scale

to learn generic features from various datasets, and transfer quite well on any other infrastructure dataset.

We also generate the segmentation heatmap using popular Grad-CAM visualization technique [43], shown in Fig. 9. It can be seen from this figure that as a *limitation*, SCNet mostly fails to detect lighter cracks with strong confidence. This in turn leads to false negatives. Few times when thin cracks do get detected, there is additional detection of a few pixels beyond the actual width of the crack, resulting in the false positives

as well.

As another visualization, we provide statistical trends on how our model performs relatively better. Fig. 10 shows the relative % of true positives classified by the 4 models being compared, on a per-dataset basis. It can be seen that our SCNet model classifies, for each of the datasets, non-trivial amount of more true positive pixels, compared to other 3 models. Similarly, Fig. 11 shows the relative % of false positives detected by the same 4 models, on a per-dataset basis. Other

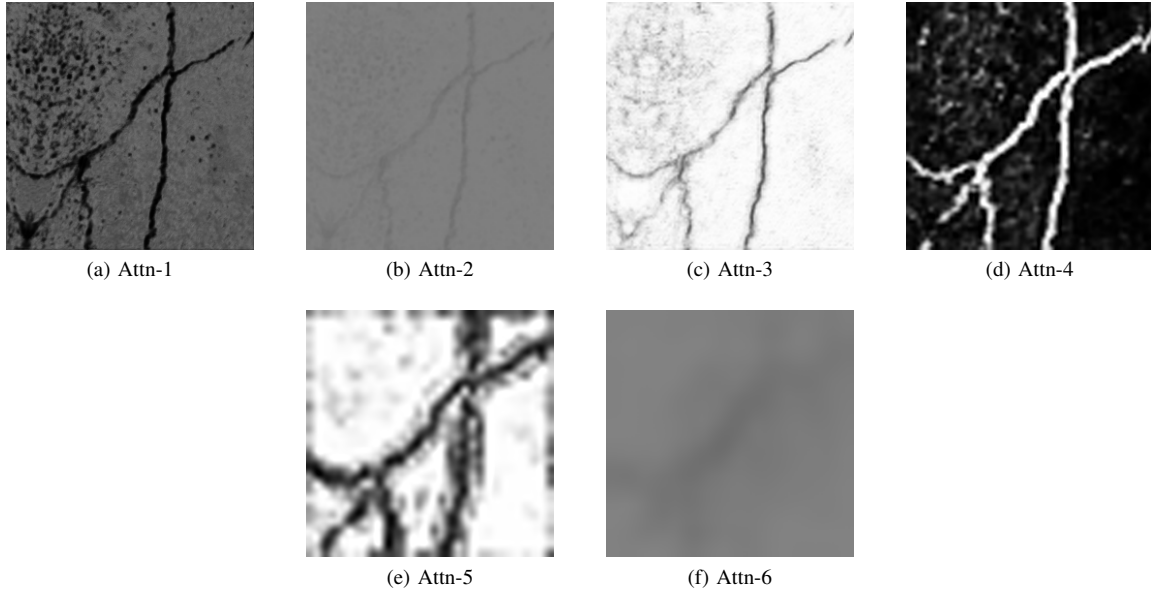


Fig. 8: Visualization of Attention Maps in Encoder Scale-space. See SCNet Architecture Diagram for Unit Names and Placements

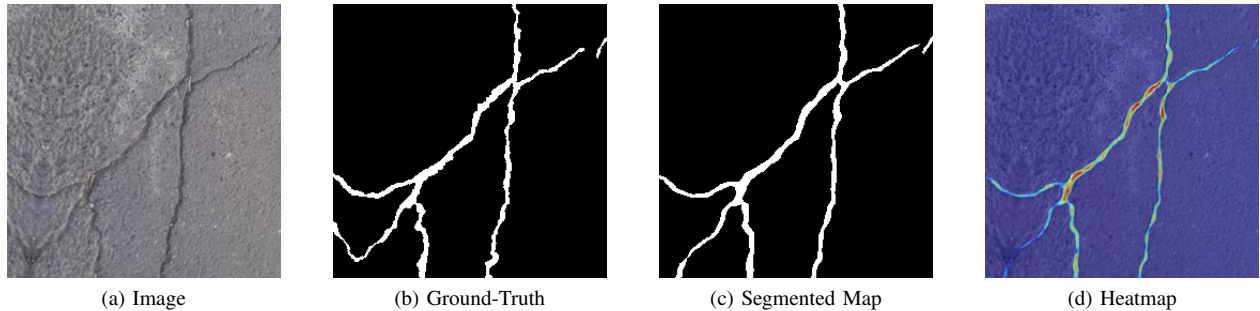


Fig. 9: Grad-CAM Heatmap Visualization of Final Prediction

than the exception of CODEBRIM dataset, for each of the remaining datasets, SCNet model classifies lesser number of false positive pixels, by a non-trivial amount. Finally, Fig. 12 shows the relative % of false negatives/missed detections by the 4 models being compared, on a per-dataset basis. Yet again, it can be seen that on each of the datasets, SCNet model misses out on lesser number of true classifications, by a non-trivial amount. All these trends point to the importance of each of the various novel elements that we have brought out in our model design, and are intuitively explained in section III. The relative importance of these elements is established in the next section, via ablation studies.

VI. EXPERIMENTS AND RESULTS ON INDUSTRIAL DATASETS

We were able to further test our model on two challenge datasets provided by BMW and Wessex Water respectively. The former dataset was based on drone-based inspection of

road networks, while the latter dataset was based on robotic inspection of interiors of a water supply pipeline/network. We did not benchmark other models (DC-1, HCNN and DC-2) on these datasets, but instead computed pixelwise F1 score and IoU score of SCNet. The results are tabulated in Tab. VI and illustrated in Figures. 14 and 15.

TABLE VI: Performance on Industrial Datasets

Dataset	Pixelwise F1 score	IoU Score
Wessex Water	98.63	93.17
BMW	94.87	90.91

VII. EXPERIMENTS AND RESULTS ON NON-INFRASTRUCTURAL DATASETS

Other than cracks in infrastructures, we were able to significantly generalize and prove the effectiveness of SCNet in two manufacturing scenarios.

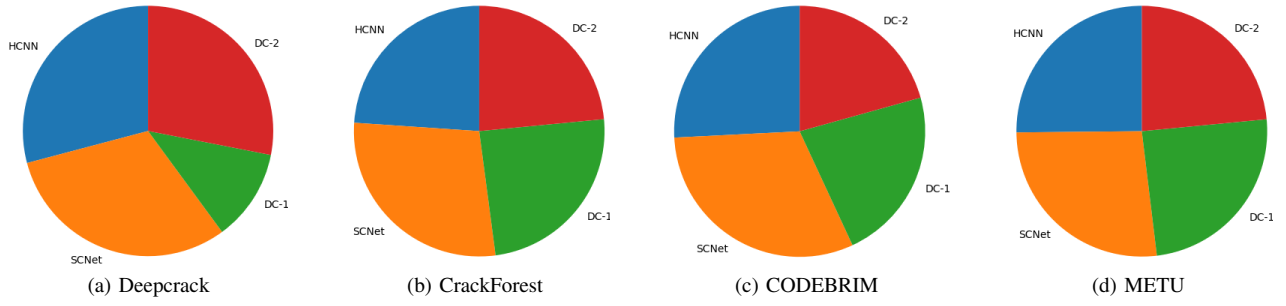


Fig. 10: Visualization of True Positives for each model, on each dataset

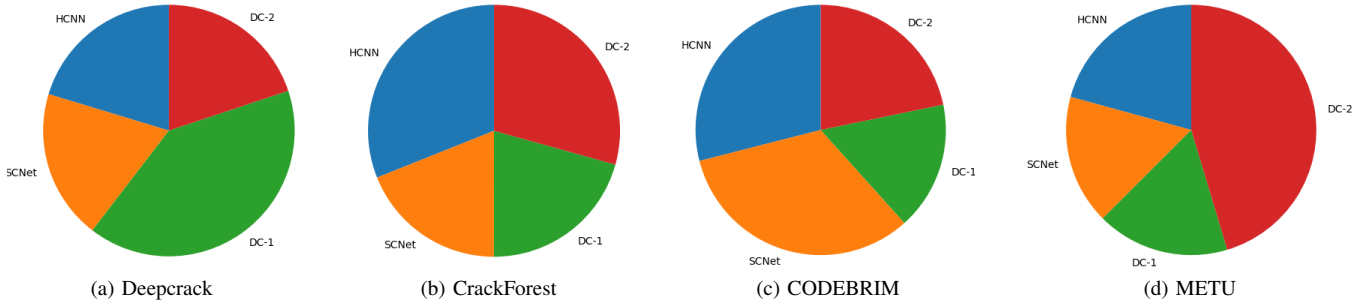


Fig. 11: Visualization of False Positives for each model, on each dataset

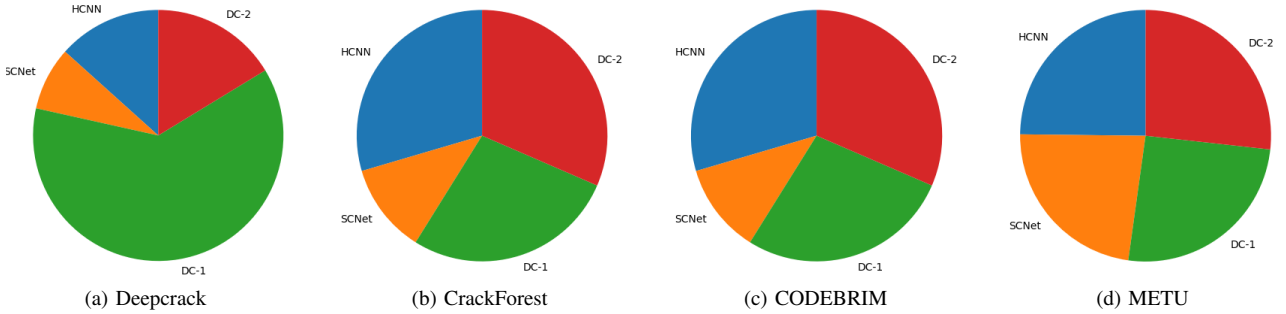


Fig. 12: Visualization of False Negatives for each model, on each dataset

A. Car Door Gap Analysis

The objective of this experiment was to check effectiveness of SCNet on predicting gaps between car doors, for quality inspections. The problem required the metric accuracy of the prediction in millimeters. The pixel-wise F1-score of SCNet for prediction came to be 95.77%, and IoU score turned out to be 91.88%, both of which are robust. Few illustrative predictions are shown in Fig. 13.

B. Steel Surfaces

We also tested our model on steel surface defects as provided in KolektorSDD2 dataset [5]. Here, only scratches resemble cracks, while SCNet is employed to predict **more than 5 other defects** as well, present in the dataset. Cumulatively, the results are encouraging: we got a pixelwise F1

score of 77.29% across all types of defects. Since defect classification is not available, we could not test for performance on segmentation of each defect in isolation. An illustrative prediction of steel surface defect is shown in Fig. 16.

VIII. ABLATION STUDIES AND DESIGN OPTIONS

We conducted extensive ablation experiments with different focuses, to understand the relative importance of model elements. These experiments cover both the aspects of any machine learning model, namely structural variations and the variations over runtime dynamics. They cover all the improvements described in section III, to establish rationality of their usage and to understand the relative advantage that they provide. Few experiments have also been conducted, to evaluate various design options. The experiments have been



Fig. 13: Illustrative Predictions of SCNet on Car Door Gaps

TABLE VII: Ablation Study on Network Architecture⁴

Dataset	Baseline		Baseline+Attn		Baseline+Attn +Focal Loss		Baseline+Attn +Focal Loss +Soft_IoU		Baseline +ScalarWeights		Baseline+Attn +Focal+Soft-Iou +Edges-1 level		Peak Performance	
	F1	Size	F1	Size	F1	Size	F1	Size	F1	Size	F1	Size	F1	Size
Deepcrack	87.56	29.46	89.27	29.46	89.98	29.46	90.57	29.46	86.91	29.46	91.91	15.30	91.23	29.46
CODEBRIM	57.92	29.46	62.65	29.46	63.28	29.46	63.60	29.46	57.79	29.46	62.69	15.30	64.22	29.46
CrackForest	79.92	29.46	86.29	29.46	87.59	29.46	88.80	29.46	79.67	29.46	90.68	15.30	90.40	29.46
METU	65.40	29.46	67.54	29.46	68.26	29.46	68.57	29.46	65.62	29.46	66.95	15.30	69.13	29.46

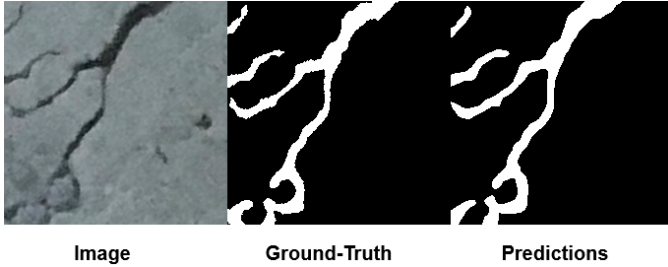


Fig. 14: Illustrative Prediction of SCNet on BMW Dataset

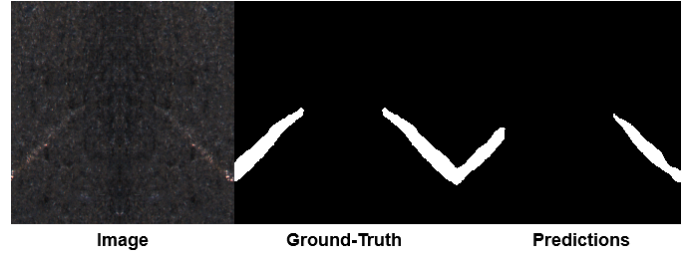


Fig. 16: Illustrative Prediction of SCNet on Multiple Steel Surface Defects

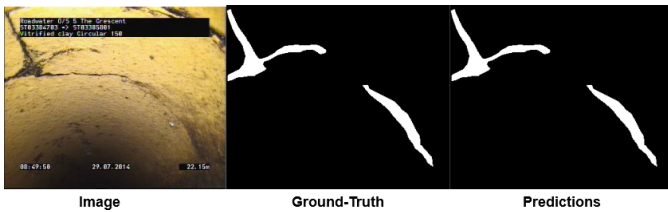


Fig. 15: Illustrative Prediction of SCNet on Wessex Water Dataset

performed on all datasets, instead of one, to make more robust inferences.

A. Architecture-related Ablations

As primary set of ablations, we studied the effect of adding/removing various units in the SCNet architecture, on its performance. This set of variations introduces a tradeoff, between the performance and the number of learnable parameters (in millions). The latter impacts the model size, which is reported as well. The effects are summarized in Table VII. In the table, the baseline corresponds to HCNN implementation,

while peak performance is based on our full model. Also, ‘ScalarWeights’ corresponds to usage of single trainable scalar instead of a filter in the attention operator, ‘Edges’ correspond to usage of 4th channel at input, while ‘-1 level’ corresponds to 4-level scale space instead of 5-level. One can see from the table that

- Among all novelties, introducing the spatial attention mechanism leads to most significant improvement in the segmentation performance, over the baseline [13], without much increase in the trainable parameters.
- Instead of using the attention module at various places, we also tried to use the trainable scalar weights for feature maps, at both the encoder and decoder side, but it did not improve the performance.
- We also tried to reduce the network complexity, using 4 scales instead of 5. As is visible in 2nd last column, the performance decreased for the more challenging datasets.
- The use of a combination of focal loss and Soft-IoU loss gives modest improvements in the segmentation performance.

TABLE VIII: Effect of Different Normalization and Pooling

Dataset	Inst. Norm. + Max Pool	Inst. Norm. + Dilated Conv
Deepcrack	91.23	90.82
CODEBRIM	64.22	62.01
METU	69.13	66.65
CrackForest	90.4	88.64

B. Loss/Optimization-related Ablations

In a complementary set of ablation experiments, we kept the architecture intact, but varied and benchmarked the dynamic behavior of the model. We first tried to initialize the model weights in different ways, to study transfer learning. We tried with standard Xavier initialization, initialization via training on a different crack dataset, and a curious (industrial) dataset having samples of surfaces and textures of various materials in everyday usage [60]. It can be seen from Table IX Xavier initialization performed the best. This implies that as another limitation, our model is currently not able to handle domain shift.

TABLE IX: Effect of Different Weight Initializations

Dataset	Xavier	Crack260	Encoder with MINC[60]
Deepcrack	91.23	90.45	86.32
CODEBRIM	64.22	62.54	49.35
METU	69.13	66.32	64.21
CrackForest	90.4	88.89	76.52

We next tried to vary the loss combinations under multi-task learning setup. We additionally tried training the model with binary cross-entropy loss as well as Lovász loss, designed for pixel-wise regression [40]. While it becomes obvious from Table X that focal loss along with Soft-IoU loss gave best performance, the impact of using soft-IoU loss additionally is modest. This can perhaps be attributed to coarser, region-level supervision provided by soft-IoU loss, as against fine-grained, pixel-level supervision provided by focal loss. As an aside, we also tried replacing max-pool with dilated convolutions, as is a popular practice today. But as Table VIII suggests, it did not yield any improvement.

TABLE X: Effect of Different Loss Formulations

Dataset	Peak Performance	CE Loss Only	CE Loss + Soft-IoU loss	Focal Loss + Lovász Loss
Deepcrack	91.23	90.53	90.73	90.15
CODEBRIM	64.22	62.83	62.87	63.28
METU	69.13	68.61	67.84	67.13
CrackForest	90.40	88.44	88.57	86.99

IX. CONCLUSION

In this paper, we have introduced a model for pixel-wise segmentation of crack faults in infrastructures. Crack faults

are one of the most critical and common faults, that can lead to failure of infrastructural systems and catastrophe. We have attempted to tackle the dual challenge of no obvious pattern across crack foreground regions, against variable and poor-textured backgrounds. We use multiple design novelties, with usage of scale-space attention in both encoder and decoder giving us the best improvement in performance. We have shown the consistency of improvement, and widespread applicability of our model, by rigorously evaluating our model against 4 infrastructure datasets of different natures and sizes. In all cases, our model outperforms the state-of-the-art by a significant margin, in terms of both F1 score and AUPRC. It was even successfully deployed and tested over two industry-provided datasets, collected in challenging conditions. Our performance improvement is without any careful tuning of hyperparameters, or post-processing. Post such enhancements, the performance of our algorithm is only bound to increase. Our work thus establishes a new baseline for the crack segmentation task. As a curious benchmarking, we could also successfully demonstrate our model’s performance in two manufacturing inspection scenarios, on vastly different anomalies. In future, to further expand its scope in manufacturing applications, we intend to more rigorously benchmark it on wide variety of *material quality inspections*, such as cracks, wrinkles, folds and scratches on leather hide, rexine cover, metal sheet etc. We are hopeful that in SCNet, we will thus be able to establish a truly generic defect segmentation model.

ACKNOWLEDGMENT

The authors gratefully acknowledge the guidance of Dr. Hiranmay Ghosh at the starting of this research work.

REFERENCES

- [1] Q. Zhou, Z. Qu, and C. Cao. Mixed Pooling and Richer Attention Feature Fusion for Crack Detection. *Elsevier Pattern Recognition Letters*, 145:96–102, 2021. 3
- [2] J. König, M. D. Jenkins, M. Mannion, P. Barrie, and G. Morison. Optimized Deep Encoder-decoder Methods for Crack Segmentation. *Elsevier Journal of Digital Signal Processing*, 108:102–109, 2021. 3
- [3] D. Dais, I. E. Bal, E. Smyrou, and V. Sarhosis. Automatic Crack Classification and Segmentation on Masonry Surfaces using Convolutional Neural Networks and Transfer Learning. *Elsevier Journal of Automation in Construction*, 125:103606, 2021. 3
- [4] X. Cui, Q. Wang, J. Dai, Y. Xue, and Y. Duan. Intelligent Crack Detection based on Attention Mechanism in Convolution Neural Network. *SAGE Journal of Advances in Structural Engineering*, pages 13–28, 2021. 3
- [5] J. Božič, D. Tabernik, and D. Skočaj. Mixed Supervision for Surface-defect Detection: from Weakly to Fully Supervised Learning. *Computers in Industry*, 2021. 11
- [6] K. Zhang, Y. Zhang, and H. Cheng. CrackGAN: Pavement Crack Detection Using Partially Accurate Ground Truths Based on Generative Adversarial Learning. *IEEE Transactions on Intelligent Transportation Systems*, pages 1–14, 2020. 3
- [7] W. Wang and C. Su. Convolutional Neural Network-based Pavement Crack Segmentation using Pyramid Attention Network. *IEEE Access*, 8:548–558, 2020. 3
- [8] J. Guo, Q. Wang, Y. Li, and P. Liu. Façade Defects Classification from Imbalanced Dataset using Meta Learning-based Convolutional Neural Network. *Computer-Aided Civil and Infrastructure Engineering*, 35(12):1403–1418, 2020. 3
- [9] C. Feng, H. Zhang, H. Wang, S. Wang, and Y. Li. Automatic Pixel-Level Crack Detection on Dam Surface using Deep Convolutional Network. *Sensors*, 20(7):2069, 2020. 2, 4

⁴Model size is in millions of parameters

- [10] Z. Dong, J. Wang, B. Cui, D. Wang, and X. Wang. Patch-based Weakly Supervised Semantic Segmentation Network for Crack Detection. *Elsevier Journal of Construction and Building Materials*, 258:120–127, 2020. [3](#)
- [11] J. Cheng, L. Ye, Y. Guo, J. Zhang, and H. An. Ground Crack Recognition Based on Fully Convolutional Network With Multi-Scale Input. *IEEE Access*, 8:53034–53048, 2020. [2](#), [3](#)
- [12] Pixel-wise annotation of codebrim. <https://drive.google.com/data-mview.html>, 2020. [6](#)
- [13] Q. Zhu, M. Phung, and Q. Ha. Crack Detection Using Enhanced Hierarchical Convolutional Neural Networks. In *Australasian Conference on Robotics and Automation*, 2019. [5](#), [7](#), [12](#)
- [14] Y. Xu, Y. Bao, J. Chen, W. Zuo, and H. Li. Surface Fatigue Crack Identification in Steel Box Girder of Bridges by a Deep Fusion Convolutional Neural Network based on Consumer-grade Camera Images. *SAGE Journal on Structural Health Monitoring*, 18(3):653–674, 2019. [2](#)
- [15] S. Park, S. Bang, H. Kim, and H. Kim. Patch-based Crack Detection in Black Box Images using Convolutional Neural Networks. *Journal of Computing in Civil Engineering*, 33(3):04019017, 2019. [3](#)
- [16] M. Mundt, S. Majumder, S. Murali, P. Panetsos, and V. Ramesh. Meta-learning Convolutional Neural Architectures for Multi-target Concrete Defect Classification with the CONcrete DEfect BRIDGE IMage dataset. In *IEEE Conference on Computer Vision and Pattern Recognition*, pages 11196–11205, 2019. [1](#), [2](#), [6](#), [7](#)
- [17] F. Locatello, S. Bauer, M. Lucic, G. Raetsch, S. Gelly, B. Schölkopf, and O. Bachem. Challenging Common Assumptions in the Unsupervised Learning of Disentangled Representations. In *International Conference on Machine Learning*, pages 4114–4124, 2019. [3](#)
- [18] Y. Liu, J. Yao, X. Lu, R. Xie, and L. Li. DeepCrack: A Deep Hierarchical Feature Learning Architecture for Crack Segmentation. *Neurocomputing*, 338:139–153, 2019. [2](#), [3](#), [6](#), [7](#)
- [19] H. Kim, E. Ahn, M. Shin, and S.-H. Sim. Crack and Noncrack Classification from Concrete Surface Images using Machine Learning. *SAGE Journal on Structural Health Monitoring*, 18(3):725–738, 2019. [3](#)
- [20] Z. Huang, X. Wang, L. Huang, C. Huang, Y. Wei, and W. Liu. CCnet: Criss-cross Attention for Semantic Segmentation. In *IEEE International Conference on Computer Vision*, pages 603–612, 2019. [3](#), [8](#)
- [21] J. Fu, J. Liu, H. Tian, Y. Li, Y. Bao, Z. Fang, and H. Lu. Dual Attention Network for Scene Segmentation. In *IEEE Conference on Computer Vision and Pattern Recognition*, pages 3146–3154, 2019. [8](#)
- [22] C. V. Dung, H. Sekiya, S. Hirano, T. Okatani, and C. Miki. A Vision-based Method for Crack Detection in Gusset Plate Welded Joints of Steel Bridges using Deep Convolutional Neural Networks. *Elsevier Journal on Automation in Construction*, 102:217–229, 2019. [2](#)
- [23] C. V. Dung et al. Autonomous Concrete Crack Detection using Deep Fully Convolutional Neural Network. *Elsevier Journal on Automation in Construction*, 99:52–58, 2019. [3](#)
- [24] Middle East Technical University Building Crack Dataset. <https://data.mendeley.com/datasets/jwsn7tfbrp/1>, 2019. [6](#), [7](#)
- [25] Q. Zou, Z. Zhang, Q. Li, X. Qi, Q. Wang, and S. Wang. Deepcrack: Learning Hierarchical Convolutional Features for Crack Detection. *IEEE Transactions on Image Processing*, 28(3):1498–1512, 2018. [3](#), [7](#)
- [26] H. Zhao, Y. Zhang, S. Liu, J. Shi, C. Change Loy, D. Lin, and J. Jia. PSAnet: Point-wise Spatial Attention Network for Scene Parsing. In *Elsevier European Conference on Computer Vision*, pages 267–283, 2018. [3](#)
- [27] X. Yang, H. Li, Y. Yu, X. Luo, T. Huang, and X. Yang. Automatic Pixel-level Crack Detection and Measurement using Fully Convolutional Network. *Computer-Aided Civil and Infrastructure Engineering*, 33(12):1090–1109, 2018. [2](#)
- [28] S. Woo, J. Park, J.-Y. Lee, and I. So Kweon. CBAM: Convolutional Block Attention module. In *Elsevier European Conference on Computer Vision*, pages 3–19, 2018. [4](#)
- [29] W. R. L. d. Silva and D. S. d. Lucena. Concrete Cracks Detection based on Deep Learning Image Classification. In *Multidisciplinary Digital Publishing Institute Proceedings*, page 489, 2018. [3](#)
- [30] S. Niklaus. A reimplement of HED using PyTorch. <https://github.com/sniklaus/pytorch-hed>, 2018. [7](#)
- [31] G. Nagendar, D. Singh, V. N. Balasubramanian, and C. Jawahar. Neuro-IOU: Learning a Surrogate Loss for Semantic Segmentation. In *British Machine Vision Conference*, pages 278–283, 2018. [4](#)
- [32] Y. Li, H. Li, and H. Wang. Pixel-wise Crack Detection using Deep Local Pattern Predictor for Robot Application. *MPDI Journal on Sensors*, 18(9):3042, 2018. [3](#)
- [33] H. Li, P. Xiong, J. An, and L. Wang. Pyramid Attention Network for Semantic Segmentation. In *British Machine Vision Conference*, page 285, 2018. [5](#)
- [34] A. Kendall, Y. Gal, and R. Cipolla. Multi-task Learning using Uncertainty to Weigh Losses for Scene Geometry and Semantics. In *IEEE Conference on Computer Vision and Pattern Recognition*, pages 7482–7491, 2018. [5](#)
- [35] H. Huang, R. He, Z. Sun, T. Tan, et al. IntroVAE: Introspective Variational Autoencoders for Photographic Image Synthesis. In *Advances in Neural Information Processing Systems*, pages 52–63, 2018. [4](#)
- [36] R. Geirhos, P. Rubisch, C. Michaelis, M. Bethge, F. A. Wichmann, and W. Brendel. ImageNet-trained CNNs are Biased towards Texture; Increasing Shape Bias improves Accuracy and Robustness. In *International Conference on Learning Representations*, 2018. [3](#)
- [37] A. Garcia-Garcia, S. Orts-Escolano, S. Oprea, V. Villena-Martinez, P. Martinez-Gonzalez, and J. Garcia-Rodriguez. A Survey on Deep Learning Techniques for Image and Video Semantic Segmentation. *Elsevier Journal on Applied Soft Computing*, 70:41–65, 2018. [3](#)
- [38] A. Doulamis, N. Doulamis, E. Protopapadakis, and A. Voulodimos. Combined Convolutional Neural Networks and Fuzzy Spectral Clustering for Real-time Crack Detection in Tunnels. In *IEEE International Conference on Image Processing*, pages 4153–4157, 2018. [2](#)
- [39] R. Davoudi, G. R. Miller, and J. N. Kutz. Structural Load Estimation using Machine Vision and Surface Crack Patterns for Shear-critical RC Beams and Slabs. *Journal of Computing in Civil Engineering*, 32(4):04018024, 2018. [2](#)
- [40] M. Berman, A. Rannen Triki, and M. B. Blaschko. The Iovász-softmax Loss: A Tractable Surrogate for the Optimization of the Intersection-over-union Measure in Neural Networks. In *IEEE Conference on Computer Vision and Pattern Recognition*, pages 4413–4421, 2018. [4](#), [13](#)
- [41] D. Zhang, Q. Li, Y. Chen, M. Cao, L. He, and B. Zhang. An Efficient and Reliable Coarse-to-fine Approach for Asphalt Pavement Crack Detection. *Elsevier Journal on Image and Vision Computing*, 57:130–146, 2017. [3](#)
- [42] C. H. Sudre, W. Li, T. Vercauteren, S. Ourselin, and M. J. Cardoso. Generalised Dice Overlap as a Deep Learning Loss function for Highly Unbalanced Segmentations. In *Deep learning in Medical Image Analysis and Multimodal Learning for Clinical Decision Support*, pages 240–248. Springer, 2017. [4](#)
- [43] R. R. Selvaraju, M. Cogswell, A. Das, R. Vedantam, D. Parikh, and D. Batra. Grad-CAM: Visual Explanations from Deep Networks via Gradient-based Localization. In *IEEE International Conference on Computer Vision*, pages 618–626, 2017. [9](#)
- [44] G. Mátyus, W. Luo, and R. Urtasun. Deeproadmapper: Extracting Road Topology from Aerial Images. In *IEEE International Conference on Computer Vision*, pages 3438–3446, 2017. [4](#), [6](#)
- [45] T.-Y. Lin, P. Goyal, R. Girshick, K. He, and P. Dollár. Focal Loss for Dense Object Detection. In *IEEE International Conference on Computer Vision*, pages 2980–2988, 2017. [4](#), [6](#)
- [46] A. W. Harley, K. G. Derpanis, and I. Kokkinos. Segmentation-aware Convolutional Networks using Local Attention Masks. In *IEEE International Conference on Computer Vision*, pages 5038–5047, 2017. [3](#)
- [47] F.-C. Chen and M. R. Jahanshahi. NB-CNN: Deep Learning-based Crack Detection using Convolutional Neural Network and Naïve Bayes Data Fusion. *IEEE Transactions on Industrial Electronics*, 65(5):4392–4400, 2017. [3](#)
- [48] Y.-J. Cha, W. Choi, and O. Büyüköztürk. Deep Learning-based Crack Damage Detection using Convolutional Neural Networks. *Computer-Aided Civil and Infrastructure Engineering*, 32(5):361–378, 2017. [3](#)
- [49] L. Zhang, F. Yang, Y. Daniel Zhang, and Y. J. Zhu. Road Crack Detection using Deep Convolutional Neural Network. In *IEEE International Conference on Image Processing*, pages 3708–3712, 2016. [3](#)
- [50] Y. Shi, L. Cui, Z. Qi, F. Meng, and Z. Chen. Automatic Road Crack Detection using Random Structured Forests. *IEEE Transactions on Intelligent Transportation Systems*, 17(12):3434–3445, 2016. [3](#), [6](#), [7](#)
- [51] M. Kampffmeyer, A.-B. Salberg, and R. Jenssen. Semantic Segmentation of Small Objects and Modeling of Uncertainty in Urban Remote Sensing Images using Deep Convolutional Neural Networks. In *IEEE Conference*

- on Computer Vision and Pattern Recognition Workshops, pages 1–9, 2016. [7](#)
- [52] X. Gibert, V. M. Patel, and R. Chellappa. Deep Multitask Learning for Railway Track Inspection. IEEE Transactions on Intelligent Transportation Systems, 18(1):153–164, 2016. [2](#)
- [53] L.-C. Chen, Y. Yang, J. Wang, W. Xu, and A. L. Yuille. Attention to Scale: Scale-aware Semantic Image Segmentation. In IEEE Conference on Computer Vision and Pattern Recognition, pages 3640–3649, 2016. [3](#)
- [54] K. Xu, J. Ba, R. Kiros, K. Cho, A. Courville, R. Salakhudinov, R. Zemel, and Y. Bengio. Show, Attend and Tell: Neural Image Caption Generation with Visual Attention. In International Conference on Machine Learning, pages 2048–2057, 2015. [3](#)
- [55] S. Xie and Z. Tu. Holistically-nested Edge Detection. In IEEE International Conference on Computer Vision, pages 1395–1403, 2015. [5](#)
- [56] K. Simonyan and A. Zisserman. Very Deep Convolutional Networks for Large-scale Image Recognition. International Conference on Learning Representations, 2015. [5](#)
- [57] T. Saito and M. Rehmsmeier. The Precision-recall plot is More Informative than the ROC Plot when Evaluating Binary Classifiers on Imbalanced Datasets. PLoS one, 10(3):0118432, 2015. [7](#)
- [58] O. Ronneberger, P. Fischer, and T. Brox. U-net: Convolutional Networks for Biomedical Image Segmentation. In Springer Conference on Medical Image Computing and Computer-assisted Intervention, pages 234–241, 2015. [3](#)
- [59] C. Koch, K. Georgieva, V. Kasireddy, B. Akinci, and P. Fieguth. A Review on Computer Vision based Defect Detection and Condition Assessment of Concrete and Asphalt Civil Infrastructure. Elsevier Journal on Advanced Engineering Informatics, 29(2):196–210, 2015. [3](#)
- [60] S. Bell, P. Upchurch, N. Snavely, and K. Bala. Material recognition in the wild with the materials in context database. In IEEE Conference on Computer Vision and Pattern Recognition, pages 3479–3487, 2015. [13](#)
- [61] W. Zhang, Z. Zhang, D. Qi, and Y. Liu. Automatic Crack Detection and Classification Method for Subway Tunnel Safety Monitoring. Sensors, 14(10):19307–19328, 2014. [2](#)
- [62] H. Lee, R. Grosse, R. Ranganath, and A. Y. Ng. Unsupervised Learning of Hierarchical Representations with Convolutional Deep Belief Networks. Communications of the ACM, 54(10):95–103, 2011. [3](#)
- [63] L. Bottou. Large-scale Machine Learning with Stochastic Gradient Descent. In Proceedings of COMPSTAT, pages 177–186. Springer, 2010. [7](#)
- [64] K. J. Dana, B. Van Ginneken, S. K. Nayar, and J. J. Koenderink. Reflectance and Texture of Real-world Surfaces. ACM Transactions On Graphics, 18(1):1–34, 1999. [3](#)